JOURNAL OF OPTOELECTRONICS AND ADVANCED MATERIALS Vol. 9, No. 12, December 2007, p. 3863 - 3870

Electrical conduction in initial field assisted sintering stages

G. ALDICA[*a], V. KHODASH[b], P. BADICA[a], J. R. GROZA[b]
[a]*National Institute of Materials Physics, Magurele, POB MG-7, RO-077125, Romania*
[b]*Division of Materials Science and Engineering, Department of Chemical Engineering and Materials Science, University of California, Davis, California 95616-5294, USA*

Field Activated Sintering Techniques (FAST) are increasingly used to consolidate metal and ceramic powders. They combine application of a pulsed electrical current with external pressure to activate the densification process. The nature of electrical field/current interaction with powder systems is not clear yet. In this regard, *in-situ* transport measurements and microstructural analyses were carried out during pulsed current application in the FAST processing of Ni powders. Our experimental results were compared with existing electrical conduction theories and observed effects were relatively well explained qualitatively within these theories. Under electrical field it was confirmed that no voltage-current phase-shift occurs at elevated operating interfacial temperatures. For the field situation a higher applied pressure is decreasing the contact instability among particles contacts and of the sintering onset temperature. Microstructural investigations of the FAST-sintered samples indicate rather distribution of the higher density regions and a considerable increase of neck formation above 340 °C.

(Received March 29, 2007; accepted December 4, 2007)

Keywords: Sintering, Electrical conduction, Ceramics

1. Introduction

Different routes have been used to get good ceramics of high uniformity and density, as e.g. soft chemistry methods [1]. Sol-gel synthesis is also recommanded [2]. A relatively new sintering techniques employing an electrical field/current application (known as Field Assisted Sintering Techniques or FAST) are currently used intensively to consolidate ceramic, metal and composite powders. These techniques combine a pulsed electrical current application to powders in a graphite die and punch unit with external pressure to activate powder densification. The assumed benefits of this activation are a uniform current path, elimination of surface contaminants, and a short densification time usually associated with minimal grain growth. Typically, FAST sintering provides higher densities in shorter times and/or lower temperatures as compared to conventional processes [3-6]. For hard sintered materials, bulk densities of above 90% of the theoretical density were easily obtained [e.g. 4,5].

FAST sintering is based on application of pulsed and DC currents through and around the specimen. Conduction along the die provides basic ohmic heating. C7onduction through the powder specimen may involve three broad classes of phenomena: constriction resistance, tunnelling and arcing [7]. In constriction resistance, the voltage drop occurs over a contact area, which is small compared to the dimensions of the powder particles. A localised area of high resistance is formed with a high corresponding Joule effect. Tunnelling or a limited conduction through a surface film occurs if film thickness is very small. Alternately, conducting paths may be created by the rupture of non-conducting surface film due to pressure. Possible arcing (with plasma generation) may take place in the vicinity of contact areas. Arcing may accommodate current transfer and is accompanied by material transfer from the cathode to the anode by high temperature local events such as melting, evaporation and re-deposition of the surface material.

One key problem of interest in FAST is the uniformity of the electric conduction in the green compact, and its implications for temperature distribution particularly in the early sintering stages. It is known that under certain combinations of applied pressure and voltage, the conduction of electricity is rather localised resulting in local melting rather than overall sintering of the compact [8,9].

The main origin of local variability comes from the statistical nature of the geometries of the contacts, i.e., different contact areas at closed contacts and gap sizes at open contacts. The size of inter-particle contacts varies significantly. As a result, concentration of the current along discrete favourable paths is possible. If the resulting localised heat cannot be effectively transferred away, a further reduction of the local resistance occurs with catastrophic effect (localised melting). In FAST, the unfavourable localisation of the electric current in the compact may be alleviated effectively with the application of pressure when the powder size is relatively large. This problem bears similarities to percolation in conductive random networks [8,10]. Additionally, the pulsed DC current applied is assumed to achieve a more uniform electric conduction through the compacted powder. The interplay/coupling between electrical current and external pressure is critical, and it has not been yet fully accounted for.

The goal of this work is to characterise the behaviour of a powder system to the combined application of a pulsed current and mechanical pressure in the initial stage of FAST sintering. The study covers the evolution of electrical conduction through metal powders associated with local and micro-structural distributions upon pressure and pulsed current application.

2. Experimental

Material

Ni powder (INCO Nickel powder type HDNP) was supplied by Novamet, N. J. Analysis of 600 particles was performed to determine the particle size and distribution using a Philips SEM 515 scanning electron microscope (SEM). SEM micrograph on the Ni powder (Fig. 1) shows the presence of only a small number of cluster of particles (between 40 and 150 μm diameter). The average diameter of the particles is 8 μm with a log-normal distribution. The particles are spherical with irregular surfaces. The particle size distribution is shown in Fig. 2 and Table 1. Using calculations presented in ref. [11] on Ni powders from the same supplier, the oxygen level is presumed to be below 500 ppm. No other impurities were detected by energy dispersive spectroscopy (EDS) measurements.

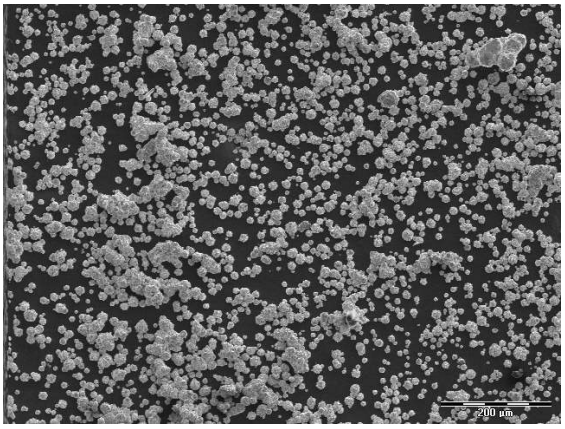

Fig. 1 SEM image on the starting Ni powder.

Table 1. Median diameter (the 50% value), tenth d_{10} and ninetieth d_{90} percentiles of the size distribution and the calculated value of surface area based on the median size for the spherical Ni particles.

Median diameter, $d_{50\%}$ (μm)	8
Tenth percentile, $d_{10\%}$ (μm)	4
Ninetieth percentile, $d_{90\%}$ (μm)	12
Surface area (m^2/g)	0.08

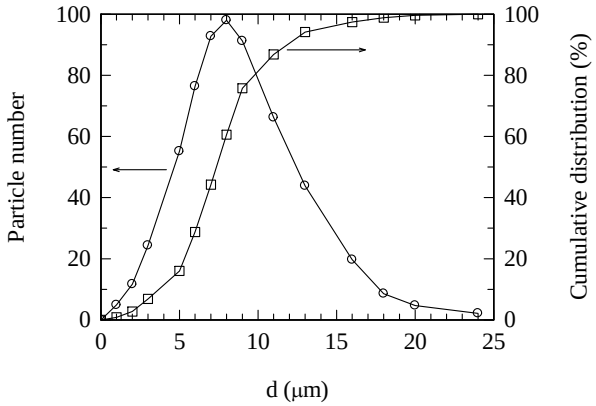

Fig. 2. Ni powder grain distribution. The clusters were not considered.

Electrical measurements

The electrical measurements were done by the four-point technique using a set-up shown in Fig. 3. The voltage-current characteristics were measured at room temperature after loading the powder into the graphite die.

The punches (0.75×1.00") and the die (0.75/1.75×1.50") were supplied by MWI Inc, Rochester, NY, USA (grade FE 250). For the acquisition of the sample voltage (U_s) two Mo wires (diameter 0.5 cm) were placed between two graphite foils (thickness = 0.13 mm) on top and bottom of the Ni powder. The resistance of the graphite foil is ≈ 15 μΩ - two orders of magnitude smaller than for the other parts of the electrical circuit. The graphite foil (0.127 mm×1 m×33 m - roll, code IGF005-40108, industrial grade foil) was supplied by Non-Metals, Inc, Tucson, AZ, USA. The wires were isolated from the punches by alumina tubes. The pressure was applied by SIMPLEX hydraulic pump.

In situ voltage measurements were done during FAST sintering in Spark Plasma Sintering (SPS) machine "Dr Sinter" (Sumitomo Coal Mining Co, Japan). FAST processing was performed in vacuum (6-15 Pa). For each experiment 10 g of Ni powder was loaded into graphite die and punch unit. The inner diameter of the die is 19 mm. A type K thermocouple measured the temperature. The hot junction of the thermocouple was placed into a horizontal channel at about 7 mm deep in the 12.7 mm thick die wall (Fig. 3). A uniaxial pressure of either 17.5 or 35 MPa was applied during sintering. The heating rates used varied between 100 and 9,900 °C/min.

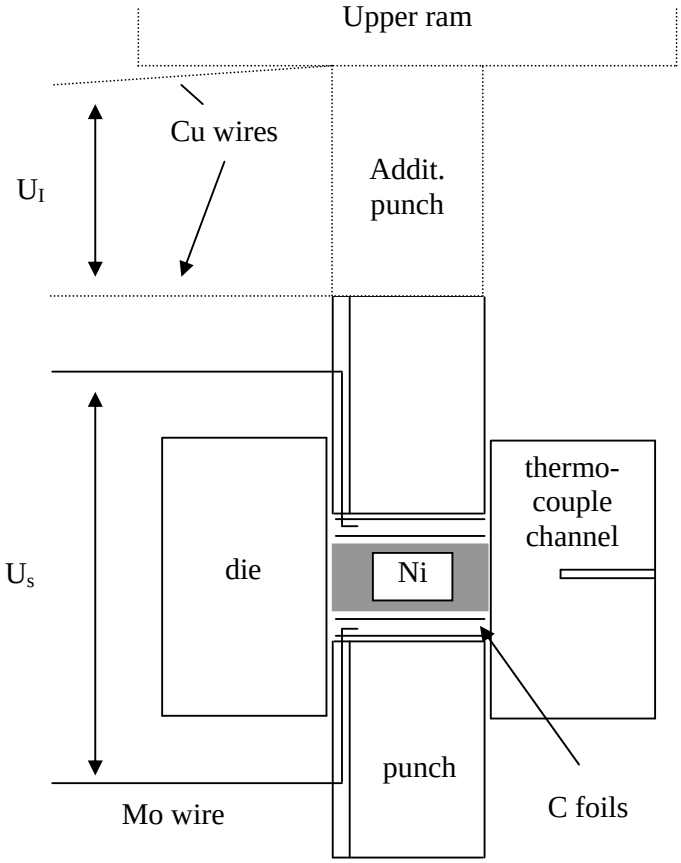

Fig. 3 Experimental set-up.

Samples and experimental conditions during FAST are shown in Table 2. Measurements on some samples (labelled Ni 9 through Ni 13) were performed using alumina tape to isolate the powders and punches from the die (in these cases we used a die with 0.80" inner diameter). This arrangement allows elimination of the contribution of the die resistance to the overall resistance of the sample (i.e., the current flows only through the punches and the sample without heating the die). The alumina tape (APA-1, 18×24×0.04" - sheet, code C4501) is from ZIRCAR Ceramics, Inc, Florida, NY, USA. Temperature of the Ni 9 - Ni 13 samples was measured by the thermocouple attached directly to the sample all the way through the channel in the die.

A HP "Infinitum" oscilloscope with two channels and memory for storage (up to 32,680 points) was used for the acquisition of data points for the current (potential drop measured on the supplement punch) and voltage values on Ni 8 – Ni 13 samples in the SPS machine. The current was determined from the measured voltage, U_I, between two Cu wires connected to a Cu foil at the top and bottom of additional punch, and the resistance of this additional punch.

The additional punch was positioned on the top the upper punch of the die-punch unit (see Fig. 3). The cooper foils (0.1 mm thickness) were used to ensure a good electric contact under the applied pressure (17.5 MPa). The resistance of the punch was measured at room temperature ($1.2 \cdot 10^{-3}$ Ω), and was calculated at a particular temperature using the function of the resistivity of graphite vs. temperature. The resistance of the punch was measured by the same technique as the sample resistance at room temperature, by substituting the sample with a dummy graphite punch. The same technique was used to measure the graphite foil resistance in the direction perpendicular to its surfaces. To obtain the current, resistance of the punch was divided by the voltage.

In the SPS apparatus we utilized a default pattern of 12:2 (on:off). The pattern of 12:2 is composed of a sequence of 12 pulses "on" and 2 pulses "off" with no current. The total time of one sequence (cycle) is about 40 ms with duration of each on/off pulse of about $3 \cdot 10^{-3}$ s. The waveform of the on-pulses is different from the square shape [12]. The operating parameters, voltage and the peak current, were below 10 V and 1000 A, respectively. The SPS machine provides shrinkage and shrinkage rate measurements. An automatic software program of the SPS machine performed data acquisition. The SPS runs were generally carried out up to about 30 seconds after the sintering onset, shown on the shrinkage rate plots.

The Ni powder was compacted in two steps: one at the room temperature by a hydraulic pump (at 24-30 MPa), and second in the SPS machine before applying the current (at the pressure specified in Table 2). The final density of the pellets was determined from geometry and weight measurements. The density was measured with a 0.1 mg Mettler Toledo balance and a 0.001 digital Mitutoyo micrometer.

The density distribution in samples was monitored by a custom made X-ray micro-tomography system. The main component is an open type micro-focus X-ray source (maximum high voltage of 160 kV at a 20 W maximum power). X-rays are detected by means of a large area, high-resolution image intensifier or amorphous silicon flat panel sensor. The scanning time varied between 2 minutes and 20 minutes. Image acquisition and 3D reconstruction were conducted by two networked Dual CPU (2GHz, 2GB RAM) Windows workstations.

3. Results and discussion

The *in situ* electrical conduction measurements during FAST (see Table 2) are shown in Figs. 4-6. Shrinkage data and microstructure of the FAST processed samples are presented in Figs. 7-9. Other current and voltage curves as well as the equivalent circuit of our experimental setup for some samples are given in Figs. 10-13.

Table 2. FAST processing conditions and final density.

Sample	Load/Pressure (kN/MPa)	T_{max} (°C)	Heating rate (°C/min)	$t_{dwelling}$ (s)	Density (g/cm^3)	Remarks
Ni 1	5/17.5	1000	200	300	7.76±0.1	SPS controller
Ni 2	5/17.5	500	100	0	5.17±0.1	SPS controller
Ni 3	5/17.5	300	100	0	4.79±0.1	SPS controller
Ni 4	10/35	300	100	0	5.03±0.1	SPS controller
Ni 5	5/17.5	415	4500	31	5.05±0.1	Manual control/NA/950 A/10 s
Ni 6	5/17.5	355	9900	32	4.97±0.1	Manual control/NA/1000 A/11 s
Ni 7	5/17.5	241	NA	17	-	SPS controller
Ni 8	5/17.5	220	400	11	4.45±0.06	SPS controller
Ni 9	5/17.5	340	NA	0	4.56±0.05	Manual control/6.0 V/480 A/4 s; Use Al_2O_3 sheet
Ni 10	5/17.5	330	NA	0	4.47±0.05	Manual control/5.4 V/1000 A/11s; Use Al_2O_3 sheet
Ni 11	5/17.5	340	NA	0	-	Manual control/5.4 V/500 A/5 s; Use Al_2O_3 sheet
Ni 12	5/17.5	510	NA	0	5.44±0.04	Manual control/6.2 V/650 A/4 s; Use Al_2O_3 sheet
Ni 13	5/17.5	100	NA	0	-	Manual control/5.2/520 A/4 s; Use Al_2O_3 sheet

Note: In *manual control* regime, the maximum voltage and the maximum current are indicated in the last column (NA - not available). Necessary time to reach these values is also presented. The information was collected through a data acquisition card (ComputerBoards PCI-DAS1200) using a LabView program. We used the graphite foils in all experiments, as shown in Fig. 3.

Before presenting our results some details of the experiments are introduced:

(a) In all experiments we measured the sample voltage using Mo wires, which were placed at the punch-sample interfaces (Fig. 3).

(b) For Ni 1-7 samples, the sample voltage was collected through a SPS data acquisition card using a LabView program.

(c) For Ni 8-13 samples, we used the oscilloscope and SPS data acquisition system. Therefore, for these samples we were doing double acquisition of the sample voltage. The current values were collected by SPS data acquisition system for all samples. In addition, for Ni 8-13 samples the voltage drop on the additional punch (Fig. 3) (used for the electrical current calculation) was acquired by the second oscilloscope channel. Therefore, in Figs. 4, 6a and 6b, the signals (the sample voltage and current data) acquired by the SPS data acquisition system are shown.

(d) In Fig. 5 we present the Ni 13 resistance calculated using the signals obtained by the two-channel oscilloscope. Ni 13 experiment took 7.5 s, when the temperature attained about 100 °C. As seen in this figure, we show the first second, after which the resistance remained flat.

(e) Although there is a carbon foil inserted between the punches and the sample (Fig. 3) we consider that contribution of the contact resistance and electrical resistance of the foil is small and only the voltage or/and the resistance of the sample is taken into account. For example, voltage U and current I curves vs. temperature for sample FAST-heated at 500 °C (Ni 2) are shown in Fig. 4.

For all FAST samples processed in the low temperature range of 100 – 300 °C (Ni 3, 4, 8) an initial peak in voltage is observed (Fig. 4). For electrical current this peak can be visualized in Fig. 10). These peaks may occur, at least partially, due to unstable contacts between the particles of the powder samples or/and instability of the automatic controller of SPS machine itself. After the voltage peak, potential-drop on the sample decreases (Fig. 4) during heating due to an increase of the number of

mechanical contacts between particles, neck growth, and cleaning the oxides from the surface of the powders (due to electro-migration effects [13] or possible plasma generation during FAST).

This decrease of the voltage (resistance) occurs in spite of the inherent increase of Ni bulk resistance with temperature. To decrease the effect of the contact instability, the applied pressure has been increased. Curves of current vs. time at two different applied pressures (Ni 2 and Ni 4) are presented in Fig. 10. The increase of applied pressure improves electrical contact between particles and therefore, likely reduces the current (and voltage) fluctuation (see curves in Fig. 10 for time > 80sec).

Using discrete element modelling techniques (i.e., a special combination of discrete element and finite element models (DE&FEM)), A. Zavaliangos et al. [9] simulated the particle packing process during FAST heating. Preliminary calculations showed that, upon heating a group of particles, the local joule heating would inevitably vary with certain statistics that reflect the stochastic nature of the powder ansambly. In these conditions, sintering rates will also vary with the faster establishing sintering contacts exhibiting more rapid decrease of electrical resistance. The resulting local temperatures also vary statistically and with a significant standard deviation (often 20-50% of the average temperature). Temperature differences over distances of the order of a

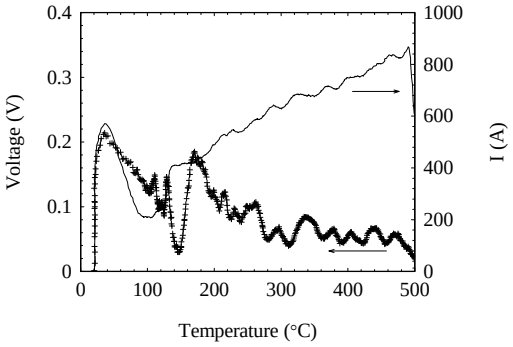

Fig. 4 Electrical parameters vs. temperature for sample heated to 500 ℃ (Ni 2): (+) voltage curve, (-) current curve.

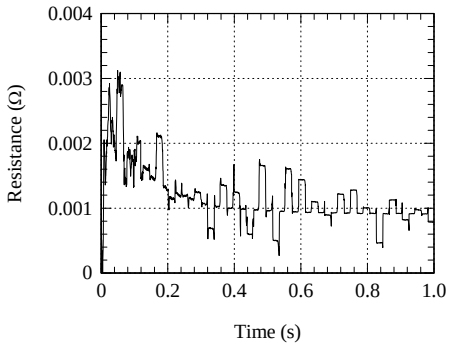

Fig. 5. R(t) curve for sample Ni 13 at the beginning of FAST process.

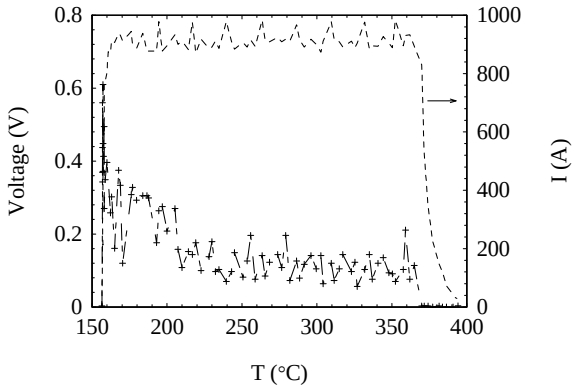

Fig. 6a. Electrical parameters vs. temperature for sample Ni 5: (+) voltage curve, (-) current curve.

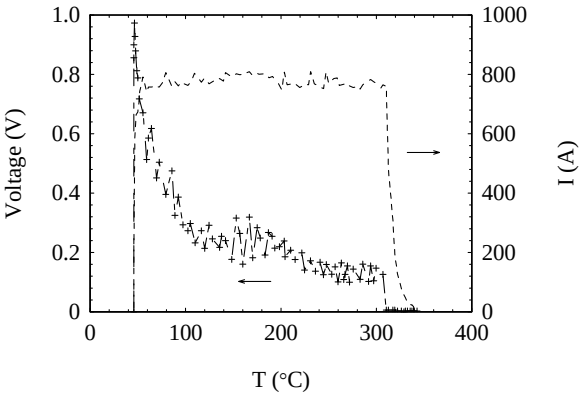

Fig. 6b. Electrical parameters vs. temperature for sample Ni 6: (+) voltage curve, (-) current curve.

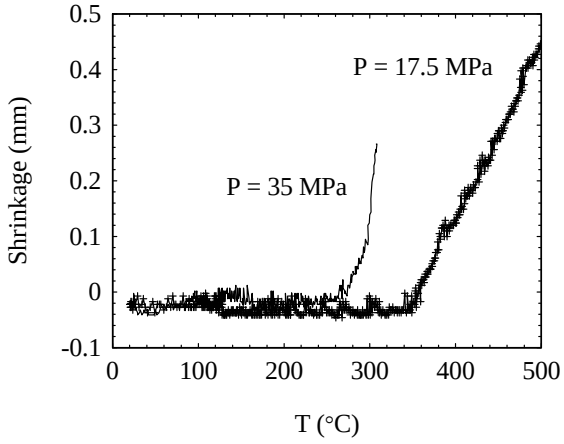

Fig. 7. Shrinkage during FAST vs. applied pressure: (Ni 2 (+++) and Ni 4 (—) samples).

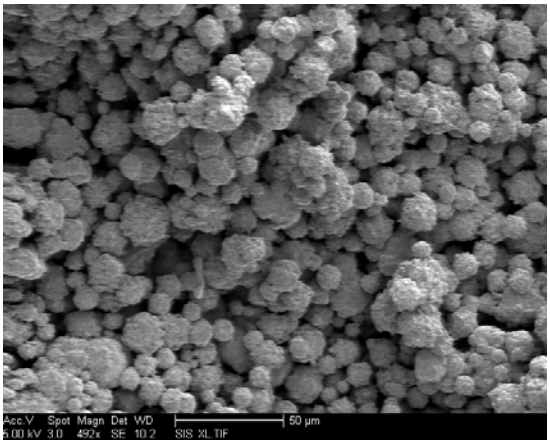

Fig. 8a. SEM images of sample heated to 220 ℃..

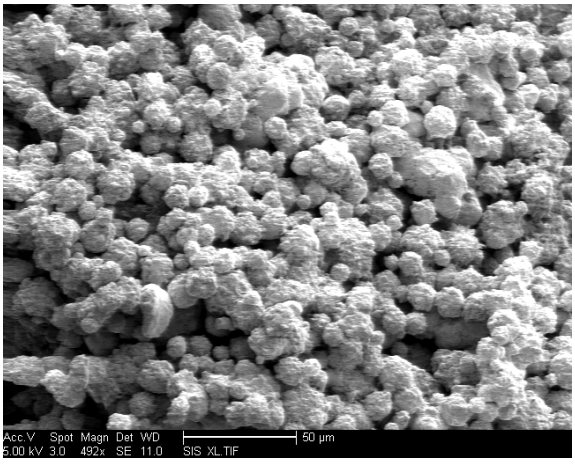

Fig. 8b. SEM images of sample heated to 340 ℃.

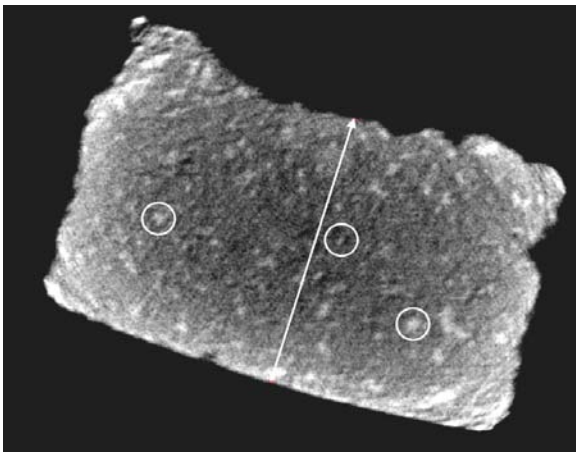

Fig. 9. μ-tomography image inside of sample Ni 8. Some clusters pointed out by the circles. The line which represents the sample breadth has 1.42 mm

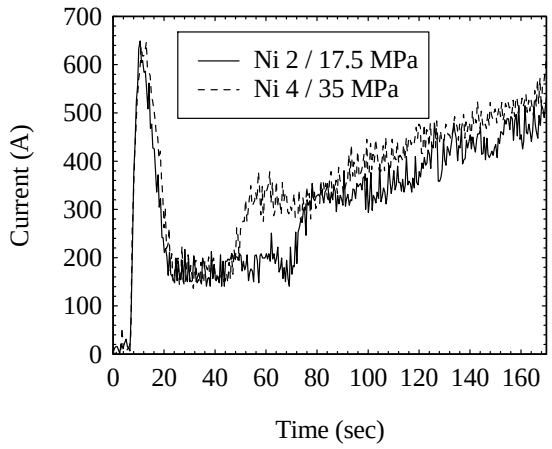

Fig. 10. The influence of the applied load on current vs. the processing time.

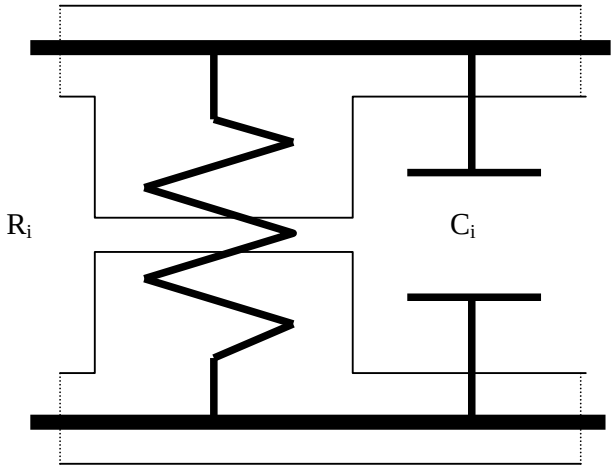

Fig. 11 Equivalent circuit of our set-up.

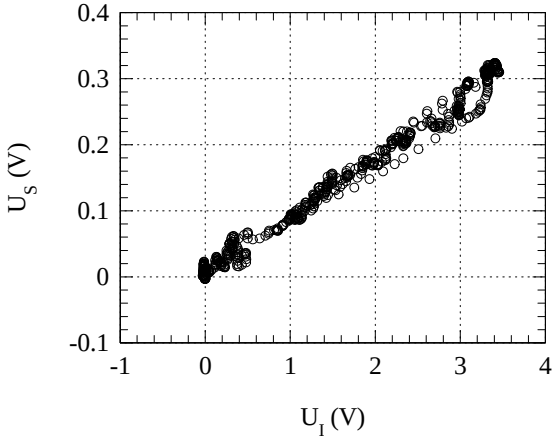

Fig. 12. $U_S - U_I$ curve for sample Ni 12 obtained from first 6 cycles.

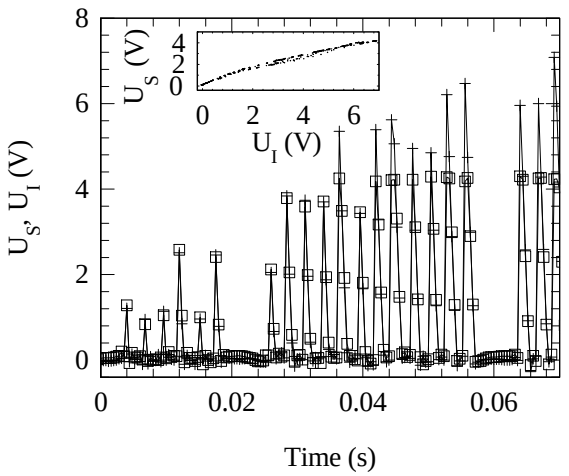

Fig. 13. Voltage vs. time dependencies for sample Ni 13: (+) from sample; (□) from punch. Inset shows U_S (U_I) curve obtained from the first 5 cycles.

multiple of the particle size results in heat transfer, which is slow due to the low thermal diffusivity of porous materials. Their results also show that the localisation of the current depends on the initial non-uniform distribution of contacts, and the initial average size of the contacts. The increase of the applied pressure results in an increase of the number of conductive paths and increases the size of contacts and, thus, the current through the compact; in Fig. 10 the current curve of sample Ni 4 pressed at 35 MPa is located at higher values than that of Ni 2 pressed at 17 MPa.

Since signal fluctuations were relatively significant (even for higher pressure of 35 MPa) a *manual control of the SPS machine* for samples Ni 5 and Ni 6 (for which pressing pressure was 17 MPa) was attempted. Indeed, smoother curves have been observed for these samples (compare Figs. 6a and 6b with Fig 4).

The manual control mode enables detection of any delay in voltage vs. current signal, if any. It may be assumed that this delay is accounted for by the reactive component of impedance in the powder system, i.e., the system has some inherent capacitance. In real powder systems, the surface of the particles is always covered with oxide films. Such systems may be assumed as being composed from a sequence of connected resistors and capacitors. If the multi-protuberance electrical contact model is considered [14] the overall impedance of the contact will be determined by the parallel connection of capacitors and resistors located at the apparent contact regions. Ideally, for independent temperature impedance, C_i, and a temperature linear resistance, R_i, for each total contact area the impedance will be given by:

$$Z = R_{load} + (R_c / (1+\omega^2 R_c C_c^2) - j\omega R_c^2 C / (1+\omega^2 R_c C_c^2), \quad (9)$$

where $C_c = \Sigma C_i$ and $R_c = 1/ \Sigma(1/R_i)$, and R_{load} is the contact bulk resistance. An equivalent circuit is shown in Fig. 11 [15]. It supports that the inter-particle contacts determine the overall impedance and cause a phase shift. Therefore, the delay in Ni powder system may be caused by the capacitance of inter-particle contacts similar to non-conductive grain boundaries in some materials [16]. Here, the possible delay in the powder system means the delay "in phase" between the sample voltage signal and the current signal measurements on additional punch.

In order to experimentally analyse the possible phase shift between voltage and current on the sample and within the described equivalent circuit an oscilloscope with two channels was used. The measuring conditions when using the oscilloscope (for samples Ni 10 – 13) are the time increment of 0.0004 s, and the sensitivity of voltage signal of 0.01 V. We note that the die is not part of the electrical circuit, because an Al_2O_3 sheet was used for the electric separation between sample and punches ansambly and the inner wall of the die (see 2.2). The measurements on Ni 12 and Ni 13 samples show no observable phase-shift in the voltage-current patterns (Figs. 12, 13). As mentioned in ref. [15], at elevated operating interfacial temperature the phase-shift drops towards zero and cannot be usually detected.

Samples were processed only at low temperatures where no shrinkage or only little shrinkage was observed. The densities of all samples were in the range 50-60 %, and only for the sample Ni 1 attained 87 % of the theoretical value of Ni (Table 2). The temperature of sintering onset depends on the applied pressure. The higher the pressure is, the lower the onset temperature of sintering (Fig. 9) is.

SEM images of fresh fracture surfaces of Ni samples sintered at 220 °C and 340 °C are presented in Figs. 8a and 8b. At 220 ^oC (Fig. 8a), the particles are barely connected. There are some clusters of particles but there is no major evidence of neck formation. In the sample sintered at 340 ^oC numerous necks between particles are noticeable (Fig. 8b).

A better account of local density distribution in the FAST-processed samples was obtained from μ-tomography. Fig. 9 indicates a few regions, rather uniformly distributed, and with higher density inside of the sample sintered at 220°C (Ni 8). The higher density areas are lighter as compared to the darker background. These areas are between 40 and 150-200 μm in size.

SEM observations on the starting Ni powder (Fig. 1) can be compared with those from the μ-tomography image on FAST processed sample (Fig. 9). The density of clusters in the starting powder was of about 7 pieces/mm^2, while in the FAST-processed sample the number of higher density areas was about 60 in a 1.4 mm x 2.4 mm area, i.e. of about 18 pieces/mm^2 (sample breadth of 1.42 mm is indicated in Fig 9). If we assume that higher density regions from the μ-tomography image are physically similar to clusters from the starting powder, it is clear that new clusters form in the FAST run given to sintering progresses.

4. Conclusions

Electrical resistance measurements were carried out on Ni powders during FAST processing before and after application of the pulsed current to characterise the response of a powder system to an applied pulsed voltage at the initial stage of sintering,

During FAST-heating, applied pressure increase was effective in decreasing the contact instability among particles and of the sintering onset temperature. In-situ voltage-current measurements during FAST revealed no voltage-current phase-shift confirming that the phase-shift drops to zero at elevated operating interfacial temperature.

SEM images of samples sintered at different temperatures showed a considerable increase of neck formation above 340 °C. The μ-tomography images inside of the samples indicate a rather uniform distribution of 40-200 μm higher density areas in the early FAST-sintering stages.

Acknowledgements

This work was performed under an NSF-DMI supported grant. One of the authors (GA) is grateful for the Research Scholar support of this work. We thank Dr. I. Tiseanu for X-ray micro-tomography measurements.

References

[1] G. Aldica, C. Plapcianu, P. Badica, C. Valsangiacom, B. Popescu, J. Optoelectron. Adv. Mater. **8**(12), 461 (2006).
[2] M. Cernea, J. Optoelec. & Adv. Mater. **7**(6), 3025 (2005).
[3] J. R. Groza, ASM Handbook, Vol. 7: Powder Metallurgy (Ohio, 1998), p. 583.
[4] O. Scarlat, S. Mihaiu, Gh. Aldica, M. Zaharescu, J. R. Groza, J. Am. Ceram. Soc. **86**, 893 (2003).
[5] J. R. Groza, J. Curtis, M. Kramer, J. Am. Ceram. Soc. **83**, 1281 (2000).
[6] V. Y. Kodash, J. R. Groza, K. C. Cho, B. R. Klotz, R. J. Dowding, Mater. Sci. & Eng. A **385**(1-2), 367 (2004).
[7] J. R. Groza, A. Zavaliangos, Mater. Sci. & Eng. A**287**, 171 (2000).
[8] J. Zhang, A. Zavaliangos, J. R. Groza, Proceeding Sintering 2003, Penn State, September 14-17, 2003.
[9] J. Zhang, A. Zavaliangos, M. Kramer, J. R. Groza, TMS Fall Meeting 2002, Columbus, Ohio, October 6-10, 2002; J. Zhang, A. Zavaliangos, M. Kramer, J. R. Groza, International Conference on Process Modeling in Powder Metallurgy & Particulate Materials, Newport Beach, California, October 28-29, 2002.
[10] A. Zavaliangos, MRS Spring Meeting, Symposium W, San Francisco, April, 3-5, 2002.
[11] R. Karmhag, G. A. Niklasson, J Appl. Phys. **85**(2), 1186 (1999).
[12] W. Chen, U. Anselmi-Tamburini, J. E. Garray, J. R. Groza, Z. A. Munir, Mater. Sci & Eng. A **394**, 132 (2005).
[13] A. G. M. Jansen, F. M. Mueller, P. Wyder, Science **199**(4333), 1037 (1978).
[14] R. W. Caven jr., J. Jalali, Proc. 37-th IEEE Holm Conf. (1991) p. 83; J. F. Archard, Proc. Roy. Soc. A **243**, 190 (1957); J. A. Greenwood, J. J. Wu, Meccanica **36**, 617 (2001).
[15] C. T. Dervos, J. M. Michaelides, IEEE Trans. Compon. Pack. A **21**(4), 530 (1998).
[16] C. A. Mead, Phys. Rev. Lett. **6**(10), 545 (1961).

*Corresponding author: aldica@infim.ro